Multicore Multimode Fiber-A New Type of Fiber Using Coupled-Core Structures

Ming-Jun Li, *Fellow, IEEE*, Kangmei Li, Xin Chen, Jeffery S. Stone, Wen Xiong, Jason E. Hurley, and Steven C. Garner

(Invited Paper)

***Abstract*—A new type of multimode fiber, multicore multimode fiber (MCMMF), which uses coupled multicore structure is proposed. The fiber has a large number of single mode cores with optimized coupling to achieve high bandwidth. A theoretical model for analyzing the MCMMF is developed. The effect of fiber parameters, such as index contrast, core radius, and core spacing on the bandwidth is systematically studied. Numerical simulations show that the bandwidth of a MCMMF can be optimized by choosing correct ratio of core spacing to core radius for a given profile design. In addition, mode coupling among the super-modes can further increase the bandwidth due to the small spacing in effective indices in coupled core structures. A MCMMF with 165 cores is fabricated. High bandwidth of 8.4 GHz·km in the 850 nm window is achieved. Using this fiber and a VCSEL-based 25 Gb/s SR transceiver, error free transmission though 150 m fiber is demonstrated.**

***Index Terms*—Coupled multicore fiber, data center, fiber bandwidth, fiber design, fiber fabrication, fiber characterization, multimode fiber.**

I. Introduction

MULTIMODE fibers (MMFs) have wide applications in short reach data transmission [1], imaging systems [2] and fiber sensors [3]. Conventional MMFs are based on a single core with a refractive index profile designed to support multiple guided modes. There are two types of profile designs for MMFs, step-index profile and graded-index profile. The refractive index of the core is higher than that of the cladding to achieve total internal reflection, which traps the light inside the core. With a step-index core that has a sharp transition, light rays traveling with different angles all reflect at the core-cladding interface. Therefore, the light rays have different optical path-lengths and different time delays compared to the graded-index design. For a graded-index core, the refractive index drops gradually from the center to the edge of the core. Light rays traveling with different angles reflect at different radial locations, which reduces the differences in path-lengths and time delays. In particular, for a certain profile shape, the optical path lengths can be equalized to minimize time delays, resulting in an MMF with high bandwidth.

High bandwidth MMF is typically designed using an alpha profile, which is defined as $n(r) = n_0 \cdot \sqrt{1 - 2\Delta(r/a)^{\alpha}}$, where n_0 is the refractive index in the center of the core, a is the core radius, and $\Delta = (n_0^2 - n_1^2)/2(n_0^2)$, where n_1 is the refractive index of the cladding [1]. When the α value is properly chosen, the modal bandwidth of the MMF can be optimized at a specific wavelength. For silica based MMFs with Germanium doped cores, the optimal alpha value is around 2.1. However, the bandwidth is very sensitive to the alpha or the profile shape. Making high bandwidth MMFs requires very accurate control of refractive index profile. With manufacturing process improvements, the modal bandwidth of commercial 50 μm core MMF for 850 nm applications has evolved from OM2 ($\geq$500 MHz·km) to OM3 ($\geq$2000 MHz·km) and to OM4 ($\geq$ 4700 MHz·km). Further improvement in bandwidth is possible through tighter profile control with more challenges in fiber manufacturing. A new type of MMF that is less sensitive to profile variations is desirable.

Recently, there has been significant research on multicore fibers (MCFs) to increase the fiber transmission capacity using the space division multiplexing (SDM) technology [4]. There are two types of MCFs: uncoupled MCFs and coupled MCFs. In an uncoupled MCF, the core spacing is large enough to ensure low crosstalk, so that each core serves as an independent transmission channel. In a coupled MCF, the core spacing is sufficiently small that each core is not independent due to crosstalk among the cores. Therefore, multiple channel transmission through a coupled MCF requires digital signal processing using MIMO technology to separate the channels. However, one advantage of coupled MCFs is that the core density is higher than uncoupled MCFs.

A coupled MCF can be considered as a new type of MMF because the interaction of the cores forms super-modes [5]. We refer this type of multicore structured multimode fiber as MCMMF. The number of super-modes is equal to the number of cores. For space division multiplexing, coupled MCFs with a small number of cores up to 12 have been investigated for SDM

Manuscript received October 3, 2019; revised November 22, 2019; accepted January 15, 2020. Date of publication January 27, 2020; date of current version February 19, 2020. This work was supported by Corning Incorporated. *(Corresponding author: Ming-Jun Li.)*

M.-J. Li, K. Li, X. Chen, J. S. Stone, J. E. Hurley, and S. C. Garner are with the Corning Incorporated, Corning, NY 14831 USA (e-mail: lim@corning.com; lik11@corning.com; chenx2@corning.com; stonejs@corning.com; hurleyje@corning.com; garnersc@corning.com).

W. Xiong is with the Facebook Reality Labs, Menlo Park, CA 94025 USA (e-mail: wenxiong@fb.com).

Color versions of one or more of the figures in this article are available online at https://ieeexplore.ieee.org.

Digital Object Identifier 10.1109/JSTQE.2020.2969564

transmission [6]–[9]. For multimode applications, the number of cores needs to be much larger, which is in the range from a few tens to a few hundreds.

We have previously proposed a new MCMMF design with large core counts and reported initial modeling and fiber results [10]. The proposed MCMMF has several potential advantages. First, the bandwidth can be high by choosing a proper core profile design and right core spacing. In addition, mode coupling plays an important role in this new type of fiber. Because the index difference between the two neighboring modes can be designed to be less than 10^{-4}, much lower than the difference of 10^{-3} of a conventional multimode fiber with 1% core delta and 50 μm core radius, the super-modes can couple to each other more easily due to various perturbations in the fiber, resulting in much higher bandwidth. The mode coupling effect can be enhanced by introducing systematic perturbations, for example, by fiber spinning during the fiber draw [11], which can further increase the bandwidth. Although the bandwidths of MCMMF that have been demonstrated so far are about 8.4 GHz·km at 850 nm, and 1.5 GHz·km at 953 nm, which are lower than the best OM4, and OM5 MMF (>10 GHz·km at 850 nm, and >3 GHz·km at 953 nm), it is expected that by optimizing the design and manufacturing process, bandwidths that meet or exceed the best OM4 and OM5 MMFs could be achieved. Second, the fiber has a large number of cores, which allows low insertion loss from a laser with large tolerance. However, for coupling to a conventional 50 μm MMF, care must be taken to reduce the insertion loss due to the core mismatch. The diameter of the core area, the core profile and the number of cores must be optimized to minimize the insertion loss. Third, the fiber could be manufactured potentially with low cost and high yield because the index profile does not need to be controlled very precisely as required in conventional graded index MMFs.

In this paper, we explore further the design space for this type of multimode fibers and present more results on fiber characteristics and transmission performance. The paper is organized as follows. Section II discusses fiber designs for MCMMF through numerical modeling using a finite element method. Section III describes fiber fabrication process and presents actual fiber characterization results. Section IV evaluates fiber transmission performance through a 25 Gb/s VCSEL-based system operating at around 850 nm and show system testing results through 100 m and 150 m of MCMMFs.

II. Fiber Designs of MCMMF

Fig. 1 shows schematically a MCMMF. It consists of multiple cores in a common cladding. The core has a diameter *d,* or a radius of *a*. The cores are separated by a distance of *D* from center to center. The multicore core region has a diameter of D_0. The fiber diameter is D_f. The relative refractive index profile of each core can be described by:

$$\Delta = \Delta_0 \left[\mathbf{1} - \left(\frac{\boldsymbol{r}}{\boldsymbol{a}} \right)^{\boldsymbol{\alpha}} \right] \tag{1}$$

where Δ_0 is the peak relative refractive index in the center of the core, a is the core radius and α is the profile shape parameter.

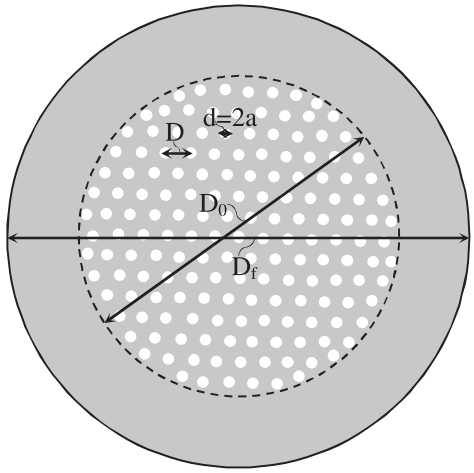

Fig. 1. Schematic of cross section of MCMMF. d: diameter of individual core; a: radius of individual core; D: core spacing; D_0: diameter of multicore area; D_f: fiber diameter.

A coupled multicore fiber supports super-modes. To design a coupled multicore fiber with high bandwidth, two conditions must be met. The first condition is that the cutoff wavelength of each core must be lower than the operating wavelength, i.e., each core is single mode at the operating wavelength. For coupled multicore fibers with single mode cores, the number of super-modes equals to the number of cores. The second condition is that coupling between the cores is just sufficiently strong to mix the modes but not too much to cause large differential group delays among the modes. The coupling coefficient depends on the overlap integral between two adjacent cores, which depends on the core design and core spacing. The coupling coefficient is designed to form super-modes with effective index differences less than 1×10^{-5}. With such low index differences, the group delay differences among the super-modes are also small, resulting in high bandwidth. In addition, with the low effective index differences, the super-modes can couple easily, which can further increase the bandwidth.

To understand characteristics of MCMMFs, we have developed a 2-D model using a finite element method. The modeling is carried out using Comsol 5.4 [12]. We choose an operating wavelength of 850 nm, at which low cost VCSEL transceivers are commercially available for data center applications. To achieve high bandwidth, each core is designed to be single mode at the operating wavelength. For a MCMMF, the core spacing affects the mode coupling strength and differential group delays (DGD). To understand the coupling between cores, a simple two-core fiber is modelled first. In the next step, we expand the model to fibers with a large number of cores.

A. Modeling of Two-Core Fibers

In the modeling, we consider four types of core designs: a step-index design with $\Delta_0 = 0.34\%$, and core radius $a = 2.6$ μm; a graded-index profile design with $\Delta_0 = 0.5\%$, $\alpha = 2.1$ and core radius $a = 3.06$ μm; a graded-index profile design with $\Delta_0 = 1\%$, $\alpha = 2.1$ and core radius $a = 2.15$ μm; and a graded-index profile design with $\Delta_0 = 1.2\%$, $\alpha = 2.1$ and core diameter $a = 1.95$ μm.

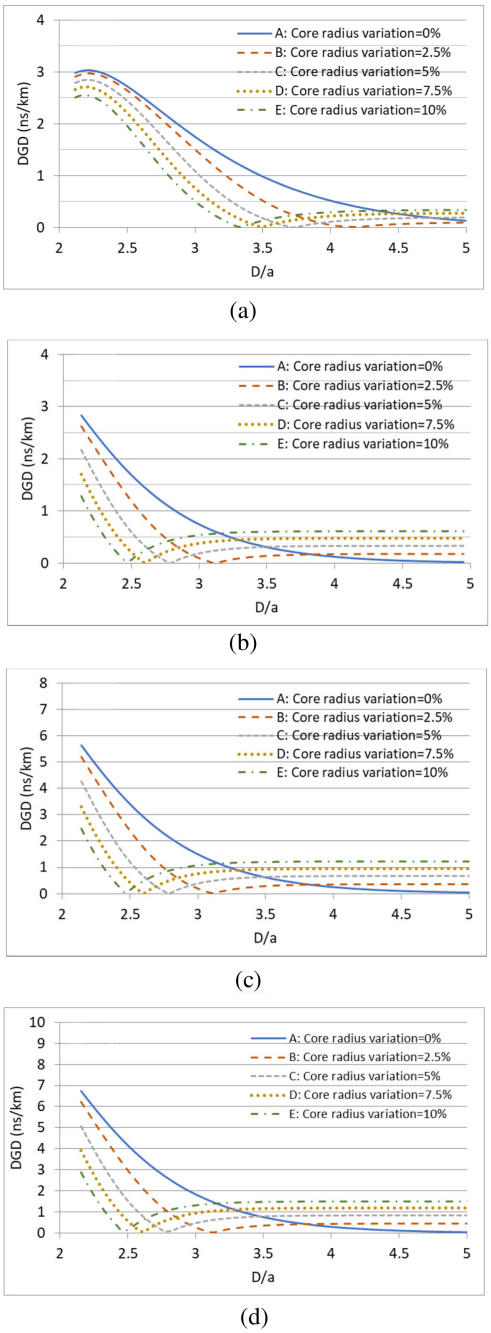

Fig. 2. Effects of core radius variation on DGD as a function of D/a for two-core fibers with four different profiles: (a) $\Delta_0 = 0.34\%$, $\alpha = 100$, and a $= 2.6\ \mu$m; (b) $\Delta_0 = 0.5\%$, $\alpha = 2.1$, and a $= 3.06\ \mu$m; (c) $\Delta_0 = 1\%$, $\alpha = 2.1$, and a $= 2.15\ \mu$m; (d) $\Delta_0 = 1.2\%$, $\alpha = 2.1$, and a $= 1.95\ \mu$m.

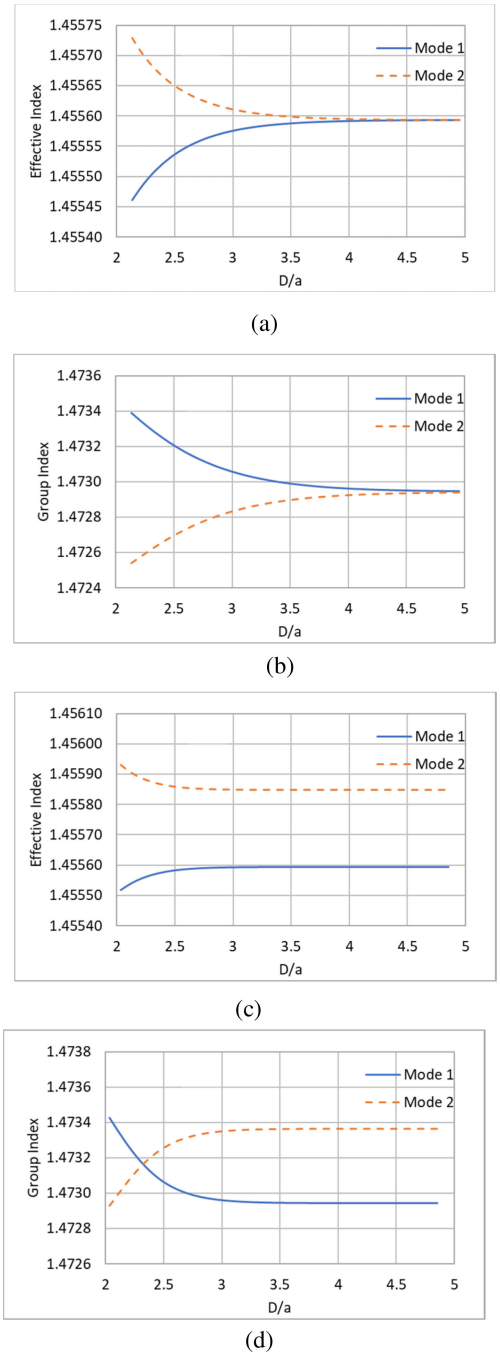

Fig. 3. Effective index and group index as a function of D/a for two core fiber with a graded index profile design with $\Delta_0 = 0.5\%$, $\alpha = 2.1$ and core radius $a = 3.06\ \mu$m. (a) and (b): without core radius variation; (c) and (d): with 5% core radius variation.

For all the four core designs, the fibers have cutoff wavelengths below 800 nm, which ensures single mode operation at 850 nm.

Fig. 2 plots the DGD as a function of the ratio of core spacing over core radius (*D/a*) for the four core index profiles. The two-core fiber supports two super-modes, a symmetric mode and an anti-symmetric mode. The two super-modes have different effective indices depending on the detailed core refractive index profile and coupling between the two cores. For identical cores, when the cores are isolated, the two super-modes have the same effective index and the group index. This is illustrated as an example in Figs. 3(a) and 3(b), where the effective index and group index are plotted as a function of *D/a* for the fiber with identical cores using the graded index profile design with $\Delta_0 = 0.5\%$, $\alpha = 2.1$ and core radius $a = 3.06\ \mu$m. For large *D/a*, DGD is near zero and the bandwidth of such a two-core fiber with identical cores can be as high as that of a single-mode fiber when the two cores are not coupled to each other. When the cores are placed sufficiently close, they start to couple. When the cores get closer, the coupling becomes stronger, resulting in

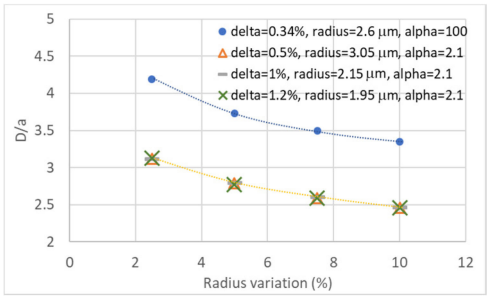

Fig. 4. D/a corresponding to minimal DGD as a function of radius variation for the four profile designs.

larger difference in effective indices and group indices between the two super-modes. The DGD follows the same trend as shown by Curves A in Fig. 2.

However, in practice it is very hard to make the two cores exactly identical. Due to variations in the fabrication process, the index contrast and the radius of cores may vary slightly. To take into account these factors, we simulated the two-core fibers with different variations of the core radius: 2.5%, 5%, 7.5% and 10%. Curves B-E of Fig. 2 plot the DGD as a function of *D/a* corresponding to the four core radius variations. These curves show that the absolute value of DGD changes with *D/a*, where *a* is the average radius of the two cores. Starting with lower value of *D/a*, the DGD decreases with *D/a* initially and then increases. When the cores are placed very close, strong coupling between the two cores results in a split of effective indices and group indices as shown in Figs. 3(c) and 3(d), similarly to what we discussed in the case with identical cores. When the cores are far apart, there is no coupling at all, and the two cores behave like two isolated single mode cores. Since the cores have different radii, the effective indices and group indices are different as shown in Figs. 3(c) and 3(d), and there is a finite DGD for the case of isolated cores. This phenomenon can be observed from the plateau of the DGD for a large *D/a* as shown in Fig. 2. The value of this DGD plateau depends on the core radius variation; the larger the variation the higher the plateau, because a larger variation increases the effective index difference between the two cores. Interestingly, the DGD reaches zero for an optimal *D/a*. At this optimal *D/a*, the DGD due the coupling between the cores and the DGD due to the core mismatch cancel each other.

The optimal *D/a* depends on the percentage of variation in core radius. A larger variation in core radius moves the optimal *D/a* to a smaller value, since stronger coupling between the cores is required to cancel the larger DGD difference due to the bigger core mismatch. Fig. 4 plots the *D/a* values corresponding to the minimal DGD for the four profile designs. It is worthwhile to note that the *D/a* values for the minimal DGD are nearly the same for the three alpha profiles that we studied, although their core deltas are different. On the other hand, the *D/a* values for the minimal DGD for the step index profile are very different from those of the alpha profiles.

We further studied effects of core delta variation on DGD of the two core fibers. Fig. 5 plots the DGD as a function of *D/a* for core delta variations from 2.5% to 10%. A similar trend

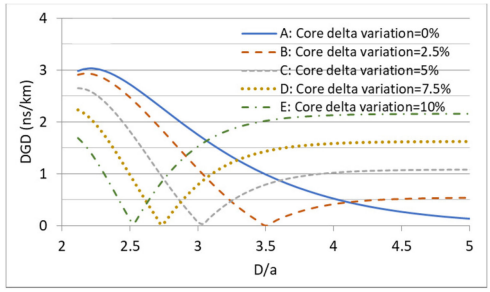

(a)

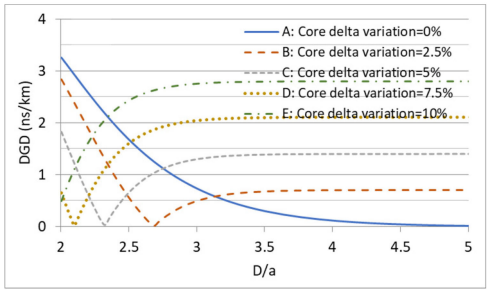

(b)

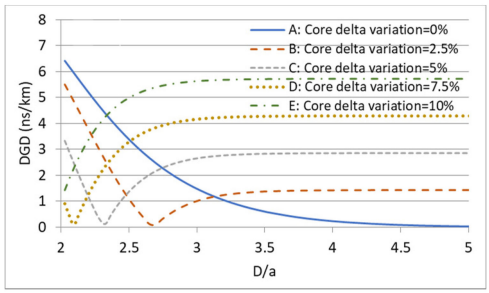

(c)

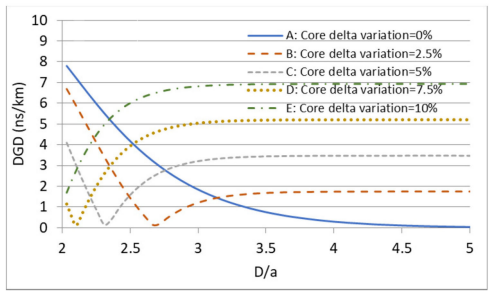

(d)

Fig. 5. Effects of core delta variation on DGD as a function of D/a for two-core fibers with four different profiles: (a) $\Delta_0 = 0.34\%$, $\alpha = 100$, and a $= 2.6$ μm; (b) $\Delta_0 = 0.5\%$, $\alpha = 2.1$, and a $= 3.06$ μm; (c) $\Delta_0 = 1\%$, $\alpha = 2.1$, and a $= 2.15$ μm; (d) $\Delta_0 = 1.2\%$, $\alpha = 2.1$, and a $= 1.95$ μm.

is observed as compared to the case of core radius variations. For a given core delta variation, there is an optimal *D/a* where the DGD reaches nearly zero. The optimal *D/a* depends on the percentage of variation in core delta, the larger the variation in core delta, the smaller the optimal *D/a* value. As shown in Fig. 6, similar to the cases with the core radius variation, we observe that the *D/a* values for the minimal DGD are nearly the same for the three alpha profiles with the same percentage of core delta

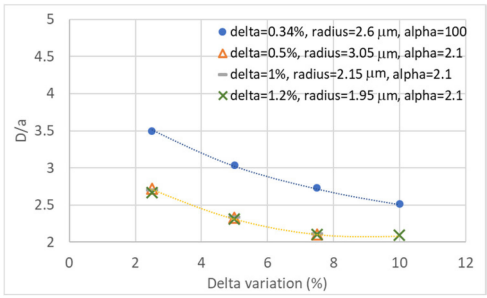

Fig. 6. D/a corresponding to minimal DGD as a function of radius variation for the four profile designs.

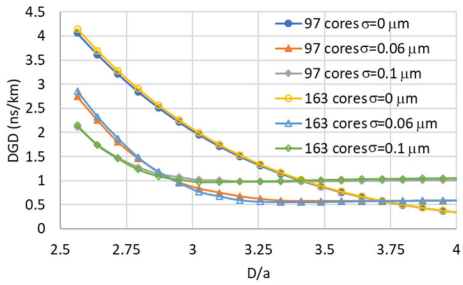

Fig. 7. DGD as a function of D/a for four fibers with numbers of cores at 97, and 163 for different standard deviations of core radius variation.

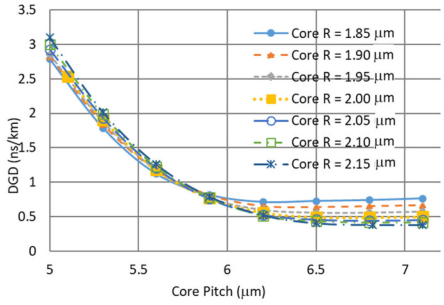

Fig. 8. DGD as a function of core pitch for 163 core fibers with several core radii.

variation, which are different from the step-index profile fiber. When the *D/a* becomes sufficiently large, the DGD reaches a plateau similarly to the cases of core radius variations. However, the DGD value at the plateau due to the core delta variation is much higher than that for case of the core radius variation. For fibers with large wavelength window of bandwidth, it is desirable to have small variation in core delta, for example less than 2.5%. On the other hand, large core delta variation results in lower value for the optimal *D/a*, which effectively increases the core density.

The results from the simple model for the coupled two-core fiber show that the core spacing is an important parameter to reduce DGD for a given core radius or index variation. The optimal spacing depends on the core design and fluctuations of core parameters in practical fibers. In practical fibers, the core radius variation is typically less than 10%, and core delta variation is typically less than 2.5%. The modeling results in Figs. 2–6 suggest that, for the core designs described earlier, a *D/a* value between about 2.5 to 3.5 can be used to minimize the DGD to get optimal bandwidth of multicore fibers with a large core count.

B. Modeling of Fibers With a Large Number of Cores

We simulated four multicore fibers containing a large number of cores of 97, 121, 139 and 163 respectively. These numbers of cores are selected according to the maximal number of cores that could fit into four circular core areas with different radii. For all the fibers, the cores have an alpha profile design with $\Delta_0 = 1.2\%$, $\alpha = 2.1$. In these fibers, the cores are arranged in a triangular lattice. The core radius follows a Gaussian distribution with an average core radius $a = 1.95$ μm and a standard deviation σ. We selected three σ values of 0, 0.06, and 0.1 μm in the simulation. Fig. 7 shows results of DGD as a function of *D/a*. It was found that for all the four core configurations, the DGD curves as a function of *D/a* are almost identical for a given σ, which suggests that for fibers with a large number of cores, the DGD versus *D/a* curves behave similarly. Therefore, we show only the two cases with the core numbers of 97 and 163 in Fig. 7. When $\sigma = 0$, which means that all the cores are identical, the DGD curves are similar to the DGD curve of the two-core fiber with identical cores as shown by Curve A in Fig. 2(d). The DGD decreases with the increase of *D/a*, reaching zero value when the cores are isolated. When the cores get closer to each other, they start to couple to form super-modes with larger difference in effective indices and group indices, which increases the DGD as explained in the two-core fiber. When the cores have variations, i.e., $\sigma \neq 0$, the DGD behavior is different from the two-core fiber. It is observed that the minimal DGD can no longer reach the zero value. Instead, the DGD reaches a low flat region when *D/a* gets sufficiently high. The starting point of the flat region depends on σ. For $\sigma = 0.06$ μm, the starting point is around 3.25; for $\sigma = 0.1$ μm, the starting point is around 2.9. Therefore, the starting point of the flat DGD region decreases with the increase of core variation. Also, the DGD value of the flat DGD region depends on the core variation. The larger the core variation is, the larger the DGD becomes. Another effect of core variation that it decreases the DGD for small *D/a* as compared with the case with no core variation.

To understand effects of the core radius on DGD, we modeled fibers with slightly different core radii. In Fig. 8, we show how DGD is evolved with the core pitch for multicore fibers with 163 cores. Similar to those fibers in Fig. 7, for all the fibers, the cores have an alpha profile design with $\Delta_0 = 1.2\%$, $\alpha = 2.1$. The curves were obtained over several different values of the average core radius ranging from 1.85 μm to 2.15 μm, with the same standard deviation $\sigma = 0.06$ μm. Again, the cores are arranged in a triangular lattice. It is found that when core pitch increases, the DGD decreases and reaches a low flat region when core pitch is roughly higher than 6 μm for all the fibers with different core radii. This corresponds to a *D/a* value range from 2.8 to 3.2, which is similar to the optimal *D/a* values obtained from the simple two-core model.

Based on the modeled DGD results in Fig. 7 and Fig. 8, it is estimated that the fiber bandwidth is about 1 to 3 GHz.km.

However, we believe that the actual fiber bandwidth can be much higher since the super-modes can couple to each other. The mode coupling effect depends on effective index differences among the super-modes. For the 163-core fiber, we calculated the effective indices of the 326 super-modes with the core radius standard deviation σ of 0.06, 0.10, 0.14, 0.18 and 0.24 μm. Modeling results do not show any meaningful trend with the standard deviation in the distribution of the effective index difference between the two neighboring modes. However, for all the five cases, 100% of the index differences between the two neighboring modes is less than 5×10^{-4}, greater than 93% of the index differences between the two neighboring modes is less than 5×10^{-5}. As a comparison, for a conventional multimode fiber with 1% core delta and 50-μm core radius, the index difference between two neighboring mode groups is about 8×10^{-3}. For such a small effective index difference, the super-modes can couple to each other easily due to various perturbations in the fiber, resulting in much higher bandwidth than the theoretical bandwidth that does not take into account the mode coupling. In particular, systematic perturbations can be introduced to the fiber, for example by fiber spinning during the fiber draw [11], which can enhance further the mode coupling effect. However, modeling the effect of mode coupling on fiber bandwidth is very complicated and we do not have a well-developed model to quantify the bandwidth improvement due to mode coupling for the MCMMF, which will be subject for future study.

C. Coupling Loss to Multimode VCSEL

For data center applications, multimode VCSEL transmitters are the central part of the cost-effective solution. The VCSEL transmitters are designed for coupling to multimode fibers with a core numerical aperture (NA) of 0.2 and a core diameter of about 50 μm. For coupling light from a VCSEL to a MCMMF with low loss, the fiber needs to have sufficient number of cores to capture the light from the laser. The coupling loss from a laser to a MCMMF can be estimated by considering the etendue conservation using the following equation:

$$\boldsymbol{IL} = -10\log\left(\frac{\boldsymbol{N}\cdot\boldsymbol{na}^2\cdot\boldsymbol{d}^2}{\boldsymbol{NA}^2\cdot\boldsymbol{D}_{\boldsymbol{L}}^2}\right) \tag{2}$$

where *na* is the numerical aperture of each core, *d* is the diameter of each core, *N* is the number of cores, *NA* is the numerical aperture of the laser, and D_L is the diameter of the laser beam. Since current VCSELs are designed for the multimode fiber with $NA = 0.2$, and $D_L = 50$ μm, we can use these numbers to estimate the insertion loss to a MCMMF. For fiber cores with the core cutoff wavelength less than 800 nm, the product of *na* and *d* needs to be less than 0.613 μm for step-index profile design. Fig. 9 shows the insertion loss from the VCSEL to a multicore fiber as a function of number of cores. For an insertion loss less than 3 dB, the number of cores needs to be 134 or higher. If the number of cores is increased to 250, the insertion loss is approaching zero. Therefore, low insertion loss can be realized by designing a fiber with a sufficiently large number of cores.

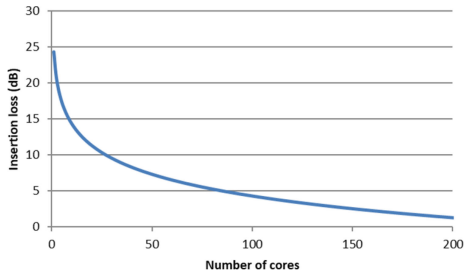

Fig. 9. Insertion loss from the VCSEL to coupled multicore fiber at 850 nm.

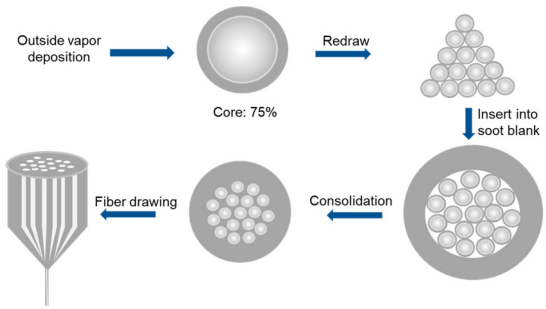

Fig. 10. Process for making MCMMF.

III. Fabrication and Characterization of MCMMF

Based on the design consideration discussed in Section II, we fabricated MCMMFs. We selected the core design with $\Delta_0 = 1.2\%$, $\alpha = 2.1$ and core radius $a = 1.95$ μm. Fig. 10 shows schematically the fabrication process. To make a MCMMF, a core preform is first made using an outside vapor deposition process (OVD) based on a core profile design. The core preform is redrawn into core canes of 2 mm in diameter. The core canes are then inserted into a silica soot blank made by OVD and consolidated into a glass multicore preform of 55 mm in diameter. The multicore preform is subsequently drawn into optical fiber using a fiber draw tower. The fiber diameter D_f was varied to scale the core radius and core spacing, which allowed us to study effects of the two parameters on fiber bandwidth.

Fig. 11(a) is the cross-section picture of the multicore fiber with 165 μm fiber diameter. The fiber has 165 cores. The cores are in a circular area with a diameter about 70 μm. Fig. 11(b) shows the statistical distribution of core radius. It follows a Gaussian distribution with an average of 1.94 μm, and a standard deviation of 0.14 μm. The average of the core spacing is 6.57 μm, and the *D/a* is 3.38.

The modal bandwidths of the MCMMFs were measured over a wavelength range from 796 nm to 980 nm using an overfill launch condition. Fig. 12 shows the measured bandwidths as a function of wavelength for fibers with 165 and 175 μm fiber diameters. For the two fibers with 175 μm, one was drawn with fiber spinning turned on, and the other one was drawn without fiber spinning. It can be seen that the fiber with spinning has higher bandwidth. The peak bandwidth is increased by about

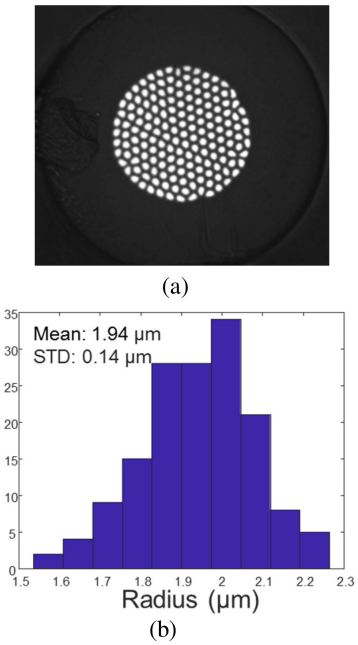

Fig. 11. (a) Multicore fiber picture. (b) Statistic distribution of core radius.

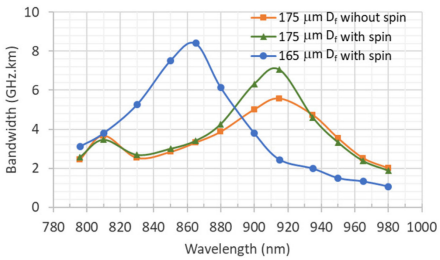

Fig. 12. Measured bandwidths as a function of wavelength for three MCMMFs.

28% with fiber spinning since the fiber spinning introduces additional mode coupling among the super-modes as discussed in Section II, resulting in lower DGD and higher bandwidth. The fiber with 165 μm fiber diameter was drawn with fiber spinning. It has a peak bandwidth of 8.4 GHz·km at 865 nm, close to the targeted peak wavelength of 850 nm. The bandwidth at 850 nm is about 7.5 GHz·km, well above the 4.7 GHz·km for OM4 MMF.

The DGD of the fiber was also measured at 850 and 953 nm at different offset positions along the diameter of the core region. Fig. 13 shows the DGD diagrams measured at 850 and 953 nm. From the DGD diagrams we observe that the temporal centroids of the pulse for both wavelengths are essentially constant across the fiber, and the output pulses are broadened due to material and modal dispersion effects. Fig. 14 shows two examples of input and output pulse profiles measured at 850 and 953 nm. A pulse shape analysis reveals that the output pulse has broadened with a near-Gaussian pulse shape similar to the shape of the input pulse. Using the full widths at half maximum of the input and output pulse, we calculated the DGD values to be 41 ps/km

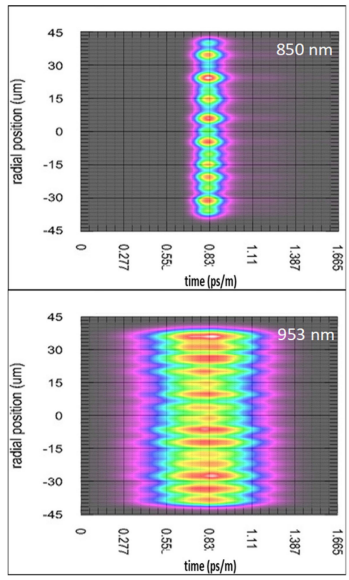

Fig. 13. Measured DGD across the fiber core area for the 165 mm diameter fiber at 850 and 953 nm.

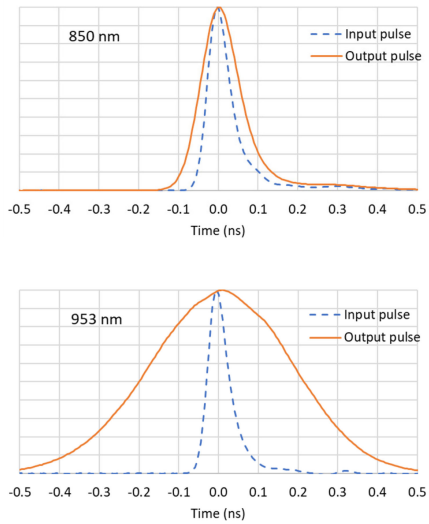

Fig. 14. Measured input and output pulse profiles for the 165 mm diameter fiber at 850 and 953 nm.

and 300 ps/km at 850 and 953 nm, respectively. Figs. 13–14 show that the output pulse at 953 nm is much broader than that at 850 nm, which explains why the measured bandwidth is lower at 950 nm as shown in Fig. 12. The DGD results indicate that the measured bandwidth of this fiber does not depend on the launch condition, which behaves differently from the conventional MMFs. This can be explained by the mode coupling effect in the fiber. When mode coupling is present, the power distribution reaches equilibrium after a short distance. Therefore, the bandwidth is independent of the launch condition. The bandwidth results suggest that the MCMMF design is highly attractive for making high bandwidth fibers for short reach applications.

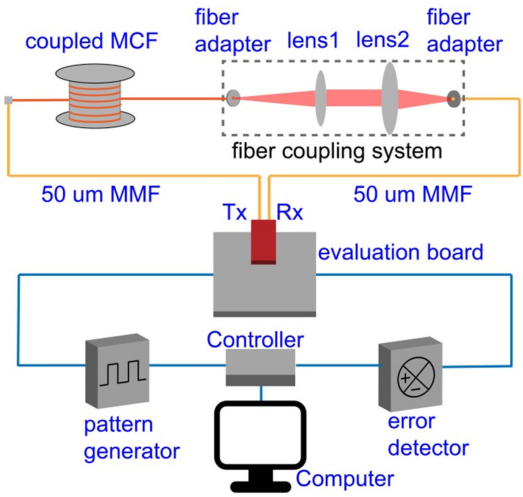

Fig. 15. Transmission system experimental setup.

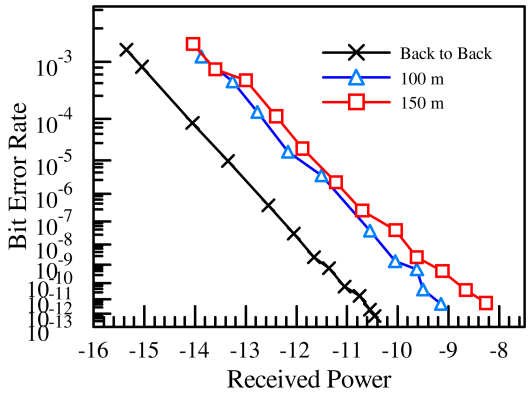

Fig. 16. The BER versus received optical power for three configurations, back to back, 100 m and 150 m of the fiber under test.

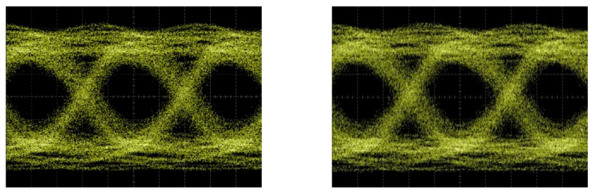

Fig. 17. Eye diagrams: (a) 100 m; and (b) 150 m coupled MCF.

IV. Transmission System Testing of MCMMF

To evaluate MCMMF transmission performance, we conducted a 25 Gb/s transmission experiment using the 165 μm diameter fiber that has high bandwidth at 850 nm and a VCSEL based transceiver.

Fig. 15 is a diagram for the transmission system setup. The transceiver is a 25 Gb/s SR transceiver (Hisense LTF8505-BC+), which is based on a multimode VCSEL. The transmitter's output optical power is -0.42 dBm. The transmission distances of this transceiver for 50 μm core MMFs are specified to be 70 m for OM3 and 100 m for OM4, respectively. As shown in Fig. 15, a conventional 50 μm core MMF is utilized as a bridge fiber, with one end connected to the coupled MCF using FC/PC connectors and the other end plugged into the transmitter. We measured the insertion loss from the 50 μm MMF to the MCMMF and vice versa. From the 50 μm MMF to the MCMMF the insertion loss is about 3.6 dB, while the insertion loss from the MCMMF to the 50 μm MMF is about 4.7 dB. Since MCMMF has a larger core around 70 μm and a different multicore design than the conventional 50 μm core MMF, the insertion loss is not symmetric from the two directions. Using the simple formula of Eq. (2), the insertion loss is estimated to be 2.1 dB, which is a little lower than the measured results. We believe the reason is that the simple formula does not take into account the light distributions in both fibers, which affect the insertion loss. To reduce the coupling loss from MCMMF to the 50 μm MMF at the receiving end, an optical coupling setup was built. The coupling setup consists of two sequential lenses mounted on a cage system, as shown in Fig. 15. We chose the focal lengths of 15.3 mm and 11.0 mm and NA of 0.16 and 0.26 for lens 1 and lens 2, respectively to optimize the coupling efficiency. The coupling system results in approximately 2.7 dB optical insertion loss. This loss number is very close to the 2.1 dB estimated from Eq. (2).

To test the system performance, an Agilent BERT system operating at 25 Gb/s was used to measure bit error rate (BER). The controller (N4960A-CJ1) controls the pattern generator (N4951B) and error detector (N4952A-E32). Using a clock signal from the error detector, the pattern generator provides 2^{31}-1 PRBS pattern that is used in our experiments. The MCMMF was prepared with two lengths of 100 m and 150 m. The BER measurements were done at fibre lengths of 1 m (back to back), 100 m and 150 m. The received optical power was adjusted by slight misalignment in the optical setup, monitored by an optical power meter. As a result, we could vary the level of optical attenuation to obtain the BER versus received optical power for the three configurations we conducted the test.

Fig. 16 shows the measured BER as a function of received power. Under the back to back condition, the system could reach error free performance at around -10.4 dBm received power. With the introduction of 100 m fibre, the system showed some power penalty, but could stay error free for 5 minutes with around -9 dBm received power. At 150 m, more power penalty showed up and the system could still achieve error free performance for 3 minutes with around -7.8 dBm received optical power. Note that 150 m is well beyond the specified distance of 100 m for OM4 MMF, benefiting from the high bandwidth of the MCMMF. We also obtained the eye diagrams for the 100 m and 150 m conditions as shown in Fig. 17, each with its maximum received power. The eye diagrams are widely open for both the 100 m and 150 m cases. It is worthwhile to note that OM4 MMF with bandwidth well above the 4.7 GHz·km bandwidth can also reach 150 m distance with the same transceiver. We conclude that the MCMMF system performance is similar to the OM4 MMF with high bandwidth.

V. Conclusions

We have proposed a new type of multimode fiber design, MCMMF using coupled multicore structures with a large core count. A theoretical model for analyzing the MCMMF is developed, which can analyze coupled multicore structures from two cores to several hundred cores. The effect of fiber parameters, such as index contrast, core radius, and core distance on the bandwidth is systematically studied. Numerical simulations show that the bandwidth of a MCMMF can be optimized by choosing correct core spacing for a given profile design. Due to the small differences in effective indices in coupled core structures, mode coupling plays an important role in this type of fiber, which can further increase the bandwidths. We have also fabricated a MCMMF with 165 cores and demonstrated high bandwidth of 8.4 GHz·km in the 850 nm window. Using this fiber and a VCSEL-based 25 Gb/s SR transceiver, error free transmission though 150 m fiber is demonstrated. With further optimization of fiber designs and manufacturing process, bandwidth can be further increased, for example greater than 10 GHz·km at 850 nm, and greater than 3 GHz·km at 953 nm, which meets or exceeds the OM5 MMF bandwidth requirements for SWDM transmission. The advantages of this MMF such as high bandwidth, simplicity in manufacturing process and large tolerance to laser coupling make it suitable for potential high data-rate short-reach communications as well as for high quality imaging transmission applications.

References

[1] M. Li, "MMF for high data rate and short length applications," in *Proc. Opt. Fiber Commun. Conf., OSA Tech. Dig. (online) (Opt. Soc. America, 2014)*, paper M3F.1.

[2] D. Psaltis, and C. Moser, "Imaging with multimode fibers," *Opt. Photon. News*, vol. 27, pp. 25–31, Jan. 2016.

[3] G. R. Jones, R. E. Jones, and R. Jones (2000) *Multimode Optical Fiber Sensors*. In: K. T. V. Grattan, B. T. Meggitt Eds., Boston, MA: Optical Fiber Sensor Technology. Springer.

[4] K. Nakajima *et al.*, "Transmission media for an SDM-based optical communication system," *IEEE Commun. Mag.*, vol. 53, no. 2, pp. 44–51, Feb. 2015.

[5] T. Sakamoto, T. Mori, M. Wada, T. Yamamoto, and F. Yamamoto, "Coupled multicore fiber design with low intercore differential mode delay for high-density space division multiplexing," *J. Lightwave Technol.*, vol. 33, no. 6, pp. 1175–1181, 2015, doi: 10.1109/JLT.2014.2376526.

[6] R. Ryf *et al.*, "Impulse response analysis of coupled-core 3-core fibers," in *Proc. Eur. Conf. Exhib. Opt. Commun., OSA Tech. Dig. (online) (Opt. Soc. America, 2012)*, paper Mo.1.F.4.

[7] T. Hayashi, Y. Tamura, T. Hasegawa, and T. Taru, "Record-low spatial mode dispersion and ultra-low loss coupled multi-core fiber for ultra-long-haul transmission," *J. Lightw. Technol.*, vol. 35, pp. 450–457, 2017.

[8] R. Ryf *et al.*, "Coupled-core transmission over 7-core fiber," in *Proc. Opt. Fiber Commun. Conf. Postdeadline Papers 2019, (Opt. Soc. America, 2019)*, paper Th4B.3.

[9] T. Sakamoto *et al.*, "Randomly-coupled single-mode 12-core fiber with highest core density," in *Proc. Opt. Fiber Commun. Conf., OSA Tech. Dig. (online) (Opt. Soc. America, 2017)*, paper Th1H.1.

[10] M. J. Li *et al.*, "High bandwidth coupled multicore fibre for data centre applications," in *45th Eur. Conf. Opt. Commun.*, (ECOC2019) Technical Digest, Paper W.3.C.6. 2019.

[11] M. J. Li and D. A. Nolan, "Fiber spin-profile designs for producing fibers with low polarization mode dispersion," *Opt. Lett.*, vol. 23, pp. 1659–1661, 1998.

[12] [Online]. Available: https://www.comsol.com/products

Ming-Jun Li (Fellow, IEEE) received the B.S. degree in applied physics from the Beijing Institute of Technology, Beijing, China, in 1983, the M.S. degree in optics and signal processing from the University of Franche-Comte, Besancon, France, in 1985, and the Ph.D. degree in physics from the University of Nice, Nice, France, in 1988. He joined Corning Incorporated in 1991 and is currently a Corporate Fellow. He has contributed to many fiber products, including bend insensitive fiber for FTTH, large effective area fiber, ultra-low PMD fiber and ultra-low loss fiber for high data rate transmission, low SBS fiber for analog transmission, high bandwidth MMF for data centers, various specialty fibers for connectors, fiber lasers, sensors and endoscopes, multicore fibers and few mode fibers for space division multiplexing, and new glass waveguide devices for optical interconnect and sensing applications. He received the 1988 French National Prize on Guided-wave Optics, and Corning's 2005 Stookey Award. He was a member of teams who won 1999 R&D 100 Award for LEAF fiber, 2008 R&D 100 Award for ClearCurve fiber, 2008 ACS Northeast Regional Industrial Innovation Award, Corning's 2016 Outstanding External Publication Award, and 2017 ACS Heroes of Chemistry Award. He was inducted into the National Inventors Hall of Fame for ClearCurve bend-insensitive optical fiber in 2020. He is a member of the National Academy of Engineering, a fellow of the IEEE society, and a fellow of the Optical Society of America. He holds 205 U.S. patents and has authored or coauthored six book chapters and more than 290 papers in journals and for conferences. He was an Associate Editor and a Coordinating Committee Member, and the Deputy Editor for the Journal of Lightwave Technology. He has also served as a Guest Editor for several special issues and as a Committee Chair or member for many international conferences.

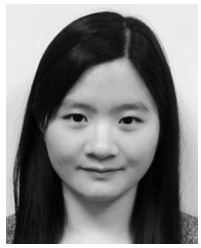

Kangmei Li received the B.S. degree in physics from Peking University, Beijing, China, in 2012 and the M.S. and Ph.D. degrees in electrical and computer engineering from Johns Hopkins University, Baltimore, MD, USA, in 2014 and 2018, respectively. She is currently a Research Scientist with Corning Incorporated, Corning, NY, USA. Her research interests include the development of ultrawide bandwidth optical devices and high-speed optical communication systems.

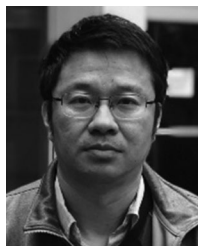

Xin Chen received the B.S. degree from Lanzhou University, Lanzhou, China, in 1991, the M.S. degree from Nankai University, Tianjin, China, in 1994, and the Ph.D. degree from Pennsylvania State University, University Park, PA, USA, in 2000, all in physics. He is currently a Research Associate with Corning Incorporated, Corning, NY, USA. His work covers several areas of optical communications, such as design and understanding of propagation effects of optical fibers, fiber measurements to transmission testing. His current research interests include short distance optical communications for data centers. He is the author of more than 100 papers published in major research journals and conferences. He is also an inventor currently holding 64 issued U.S. patents. He has served in Optical Fiber Communication Conference as a Committee Member of Fibers and Optical Propagation Effects committee from 2008 to 2011 and as an Associate Editor for Journal of Lightwave Technology from 2011 to 2014. He has been a TPC Member of OECC/PSC 2019, Cat. O3: Optical Fibers, Cables and Fiber Devices and is currently serving as a TPC Member of Optical Fiber Communication Conference 2020 Subcommittee D4: Fibers and Optical Propagation Physics.

Jeffery S. Stone received the A.S. degree from Corning Community College, Corning, NY, USA, in 1987. He joined Corning Incorporated in 1997 and is currently an Optical Scientist-Distinguished Associate. He has been working on research and development of new novel optical fibers for long haul and submarine applications as well data center applications and numerous other specialty fiber applications throughout his 22-year career. He is the coauthor of 23 publications in journals and conferences and a Co-Inventor of nine U.S. patents.

Wen Xiong received the Bachelor of Engineering degree in optical engineering from Zhejiang University, Hangzhou, China, in 2013, and the Ph.D. degree in applied physics from Yale University, New Haven, CT, USA, in 2019. She is an Optical Scientist with Facebook Reality Labs.

Jason E. Hurley received the Associates of Applied Science degree in electronics technology from the Pennsylvania College of Technology, Williamsport, PA, USA, in 1996 and the Bachelor of Science degree in electrical engineering from Alfred University, Alfred, NY, USA, in 2008. He joined Corning Inc., in the Science and Technology Division, in 1997. He is a Senior Scientist with the Optical & Wireless Transmission group, focusing on fiber characteristics to improve system performance on single mode and multimode fibers. He has coauthored more than 50 journals and conference articles and has eight patents in the field of optical communications.

Steven C. Garner received the B.S. degree in electrical engineering from Alfred University, Alfred, NY, USA, in 2007. Since 2000, he has been leading the optical measurements team at Corning Incorporated's Center for Fiber-Optic Testing, focusing on product performance, as well as new product development, commercial introductions, and application engineering. He has been an active contributor to optical fiber international measurement standards and is focused on multimode optical fiber measurements and systems.